NUMERICAL STUDY OF ION ACCELERATION AND PLASMA JET FORMATION IN THE INTERACTION OF AN INTENSE LASER BEAM NORMALLY INCIDENT ON AN OVERDENSE PLASMA: A VLASOV CODE SIMULATION

Magdi Shoucri

Institut de Recherche Hydro-Québec (IREQ), Varennes, Canada

The relevant equations

Time *t* is normalized to the inverse electron plasma frequency ω_{pe}^{-1}, length is normalized to $l_0 = c\omega_{pe}^{-1}$, velocity and momentum are normalized respectively to the velocity of light *c* and to $M_e c$. The general form of the Vlasov equation in a 4D phase-space for the electron distribution function $F_e(x, p_{xe}, p_{ye}, p_{ze}, t)$ and the ion distribution function $F_i(x, p_{xi}, p_{yi}, p_{zi}, t)$ (one spatial dimension) is written in a dimensionless form as follows :

$$\frac{\partial F_{e,i}}{\partial t} + m_{e,i}\frac{p_{xe,i}}{\gamma_{e,i}}\frac{\partial F_{e,i}}{\partial x} \mp (\vec{E} + \frac{\vec{p}\ \mathrm{x}\ \vec{B}}{\gamma_{e,i}}) \cdot \frac{\partial F_{e,i}}{\partial \vec{p}_{e,i}} = 0 \qquad \textbf{(1)}$$

with $\gamma_{e,i} = \left(1 + m_{e,i}^2 (p_{xe,i}^2 + p_{ye,i}^2 + p_{ze,i}^2)\right)^{1/2}$ **(2)**

(the upper sign in (1) is for the electrons equation and the lower sign for the ions equation, and subscripts *e* or *i* denote electrons or ions respectively). In our normalized units $m_e = 1$ **and** $m_i = \frac{M_e}{M_i}$**, the ratio of electron to ion masses.**

We write the hamiltonian of a particle in the electromagnetic field of the wave:

$$H_{e,i} = \frac{1}{m_{e,i}}(\gamma_{e,i} - 1) \mp \varphi . \qquad \textbf{(3)}$$

where φ is the scalar potential. Equation (1) can be reduced to a two-dimensional pha ıce Vlasov equation as follows. The canonical momentum $\vec{P}_{ce,i}$ is connected to the parti mentum $\vec{p}_{e,i}$ by the relation $\vec{P}_{ce,i} = \vec{p}_{e,i} \mp \vec{a}$. $\vec{a} = e\vec{A}/M_e c$ is the normalized vector potent ɔm Eqs.(2) and (3), we can write:

$$H_{e,i} = \frac{1}{m_{e,i}}\left(\left(1 + m_{e,i}^2 (\vec{P}_{ce,i} \pm \vec{a})^2\right)^{1/2} - 1 \right) \mp \varphi . \qquad \textbf{(4)}$$

Choosing the Coulomb gauge ($div\vec{a}=0$) , we have for our 1D problem $\frac{\partial a_x}{\partial x}=0$, hence $a_x=0$. The vector potential is now $\vec{a}=\vec{a}_\perp(x,t)$, and we also have the following relation along the longitudinal direction:

$$\frac{dP_{cxe,i}}{dt}=-\frac{\partial H_{e,i}}{\partial x} \qquad \textbf{(5)}$$

And since there is no transverse dependence:

$$\frac{d\vec{P}_{c\perp e,i}}{dt}=-\nabla_\perp H_{e,i}=0. \qquad \textbf{(6)}$$

This last equation means $\vec{P}_{c\perp e,i}=$const. We can choose this constant to be zero without loss of generality, which means that initially all particles at a given *(x,t)* have the same perpendicular momentum $\vec{p}_{\perp e,i}=\pm\vec{a}_\perp(x,t)$. The Hamiltonian now is written:

$$H_{e,i}=\frac{1}{m_{e,i}}\left(\left(1+m_{e,i}^2p_{xe,i}^2+m_{e,i}^2a_\perp^2(x,t)\right)^{1/2}-1\right)\mp\varphi(x,t). \qquad \textbf{(7)}$$

The 4D distribution function $F_{e,i}(x,p_{xe,i},\vec{p}_{\perp e,i},t)$ can now be reduced to a 2D distribution function $f_{e,i}(x,p_{xe,i},t)$:

$$F_{e,i}(x,p_{xe,i},\vec{p}_{\perp e,i},t)=f_{e,i}(x,p_{xe,i},t)\delta(\vec{p}_{\perp e,i}\mp\vec{a}_\perp). \qquad \textbf{(8)}$$

$f_{e,i}(x,p_{xe,i},t)$ **verify the relation:**

$$\frac{df_{e,i}}{dt}=\frac{\partial f_{e,i}}{\partial t}+\frac{\partial H_{e,i}}{\partial p_{xe,i}}\frac{\partial f_{e,i}}{\partial x}-\frac{\partial H_{e,i}}{\partial x}\frac{\partial f_{e,i}}{\partial p_{xe,i}}=0. \qquad \textbf{(9)}$$

Which gives the following Vlasov equations for the electrons and the ions::

$$\frac{\partial f_{e,i}}{\partial t}+m_{e,i}\frac{p_{xe,i}}{\gamma_{e,i}}\frac{\partial f_{e,i}}{\partial x}+(\mp E_x-\frac{m_{e,i}}{2\gamma_{e,i}}\frac{\partial a_\perp^2}{\partial x})\frac{\partial f_{e,i}}{\partial p_{xe,i}}=0. \qquad \textbf{(10)}$$

where $\gamma_{e,i}=\left(1+\left(m_{e,i}p_{xe,i}\right)^2+\left(m_{e,i}a_\perp\right)^2\right)^{1/2}$.

$$E_x=-\frac{\partial\varphi}{\partial x} \quad \textbf{and} \quad \vec{E}_\perp=-\frac{\partial\vec{a}_\perp}{\partial t} \qquad \textbf{(11)}$$

and Poisson's equation is given by:

$$\frac{\partial^2 \varphi}{\partial x^2} = \int f_e(x, p_{xe}) dp_{xe} - \int f_i(x, p_{xi}) dp_{xi} \qquad \textbf{(12)}$$

The transverse electromagnetic fields E_y, B_z **and** E_z, B_y **for the circularly polarized wave obey Maxwell's equations. With** $E^{\pm} = E_y \pm B_z$ **and** $F^{\pm} = E_z \pm B_y$**, we have:**

$$(\frac{\partial}{\partial t} \pm \frac{\partial}{\partial x})E^{\pm} = -J_y \textbf{.} \ \textbf{;} \qquad (\frac{\partial}{\partial t} \mp \frac{\partial}{\partial x})F^{\pm} = -J_z \qquad \textbf{(13)}$$

Which are integrated along their vacuum characteristic *x=t*. In our normalized units we have the following expressions for the normal current densities:

$$\vec{J}_{\perp} = \vec{J}_{\perp e} + \vec{J}_{\perp i} \ ; \qquad \vec{J}_{\perp e,i} = -\vec{a}_{\perp} m_{e,i} \int_{-\infty}^{+\infty} \frac{f_{e,i}}{\gamma_{e,i}} dp_{xe,i} \textbf{.} \qquad \textbf{(14)}$$

The numerical scheme

Since the early works presented in [8,9] which proposed the second-order fractional step scheme for the solution of the Vlasov-Poisson system, the direct solution of the Vlasov equation as a partial differential equation in phase-space has become an important method for the numerical solution of the Vlasov equation (see the review articles in [11,12]). The code we use applies a numerical scheme based on a two-dimensional advection technique, of second order accuracy in time-step, where the value of the distribution function is advanced in time by interpolating in two dimensions along the characteristics using a tensor product of cubic *B*-splines [13,14], also called an Euler-Lagrange method [15].

The numerical scheme to advance equation (10) from time t_n to t_{n+1} necessitates the knowledge of the electromagnetic field $E^{\pm}$ and $F^{\pm}$ at time $t_{n+1/2}$. This is done using a centered scheme where we integrate (13) exactly along the vacuum characteristics with $\Delta x = \Delta t$, to calculate $E^{\pm n+1/2}$ and $F^{\pm n+1/2}$ as follows:

$$E^{\pm}(x \pm \Delta t, t_{n+1/2}) = E^{\pm}(x, t_{n-1/2}) - \Delta t J_y(x \pm \Delta t/2, t_n) \qquad \textbf{(15)}$$

with $J_y(x \pm \Delta t/2, t_n) = \dfrac{J_y(x \pm \Delta x, t_n) + J_y(x, t_n)}{2}$

A similar equation can be written for $F^{\pm n+1/2}$. From (11) we also have $\vec{a}_{\perp}^{n+1} = \vec{a}_{\perp}^{n} - \Delta t \vec{E}_{\perp}^{n+1/2}$, from which we calculate $\vec{a}_{\perp}^{n+1/2} = (\vec{a}_{\perp}^{n+1} + \vec{a}_{\perp}^{n})/2$. To calculate $E_x^{n+1/2}$, two methods have been used. A first method calculates E_x^n from $f_{e,i}^n$ using Poisson's equation, then we use a Taylor expansion::

$$E_x^{n+1/2} = E_x^n + \frac{\Delta t}{2}\left(\frac{\partial E_x}{\partial t}\right)^n + 0.5\left(\frac{\Delta t}{2}\right)^2\left(\frac{\partial^2 E_x}{\partial t^2}\right)^n;$$

$$\text{with } \left(\frac{\partial E_x}{\partial t}\right)^n = -J_x^n; \qquad \left(\frac{\partial^2 E_x}{\partial t^2}\right)^n = -\left(\frac{\partial J_x}{\partial t}\right)^n. \qquad \textbf{(16)}$$

and $J_x^n = m_i \int_{-\infty}^{+\infty} \frac{p_{xi}}{\gamma_i} f_i^n dp_{xi} - m_e \int_{-\infty}^{+\infty} \frac{p_{xe}}{\gamma_e} f_e^n dp_{xe}$

A second method to calculate $E_x^{n+1/2}$ **is to use Ampère's equation:** $\frac{\partial E_x}{\partial t} = -J_x$**, from which** $E_x^{n+1/2} = E_x^{n-1/2} - \Delta t J_x^n$**. Both methods gave the same results. (We have used this second method for the results presented in section 3).**

Equation (10) is solved using an Euler-Lagrange scheme. Given $f_{e,i}^n$ **at mesh points (we stress here that the subscript *i* denotes the ion distribution function), we calculate the new value** $f_{e,i}^{n+1}$ **at the grid points j_x , and** j_p **corresponding to the mesh points** (x_{j_x}, p_{xe,ij_p}) **by writing that the distribution function is constant along the characteristics. The characteristics equations for (10) are given by:**

$$\begin{aligned} \frac{dx}{dt} &= m_{e,i} \frac{p_{xe,i}}{\gamma_{e,i}} = V_{xe,i}(x, p_{xe,i}) \\ \frac{dp_{xe,i}}{dt} &= \mp E_x - \frac{m_{e,i}}{2\gamma_{e,i}} \frac{\partial a_\perp^2}{\partial x} = V_{p_{xe,i}}(x, p_{xe,i}) \end{aligned} \quad . \qquad \textbf{(17)}$$

We assume that at the time $t_{n+1} \equiv t_n + \Delta t$ **, x is at the grid point j_x , and** $p_{xe,i}$ **is at the grid point j_p . The following leapfrog scheme can be written for the solution of (17):**

$$\frac{x_{j_x} - x(t_n)}{\Delta t} = V_{xe,i}(x^{n+1/2}, p_{xe,i}^{n+1/2}) = V_{xe,i}\left(\frac{x_{j_x} + x(t_n)}{2}, \frac{p_{xe,ij_p} + p_{xe,i}(t_n)}{2}\right) \quad . \qquad \textbf{(18)}$$

$$\frac{p_{xe,ij_p} - p_{xe,i}(t_n)}{\Delta t} = V_{p_{xe,i}}(x^{n+1/2}, p_{xe,i}^{n+1/2}) = V_{p_{xe,i}}\left(\frac{x_{j_x} + x(t_n)}{2}, \frac{p_{xe,ij_p} + p_{xe,i}(t_n)}{2}\right) \quad . \qquad \textbf{(19)}$$

where $(x(t_n), p_{xe,i}(t_n))$ **is the point where the characteristic is originating at** t_n **(not necessarily a grid point).**

Put $\Delta_{xe,i} = \frac{x_{j_x} - x(t_n)}{2}$; $\Delta_{p_{xe,i}} = \frac{p_{xe,ij_p} - p_{xe,i}(t_n)}{2}$**.** **(20)**

Equations (18) and (19) can be rewritten as:

$$\Delta_{xe,i} = \frac{\Delta t}{2} V_{xe,i}(x_{j_x} - \Delta_{xe,i}, p_{xe,ij_p} - \Delta_{p_{xe,i}}) . \quad \textbf{(21)}$$

$$\Delta_{p_{xe,i}} = \frac{\Delta t}{2} V_{p_{xe,i}}(x_{j_x} - \Delta_{xe,i}, p_{xe,ij_p} - \Delta_{p_{xe,i}}) . \quad \textbf{(22)}$$

Which are implicit equations for $\Delta_{xe,i}$ and $\Delta_{p_{xe,i}}$ and are solved by iteration. This iteration is effected as follows. We rewrite (21,22) in the vectorial form:

$$\Delta_{\mathbf{X}e,i} = \frac{\Delta t}{2} \mathbf{V}_{e,i}(\mathbf{X}_{e,i} - \Delta_{\mathbf{X}e,i}, t_{n+1/2}) \ . \quad \textbf{(23)}$$

$\mathbf{X}_{e,i}$ is the two dimensional vector $\mathbf{X}_{e,i} = (x, p_{xe,i})$, and $\Delta_{\mathbf{X}e,i} = (\Delta_{xe,i}, \Delta_{p_{xe,i}})$ is the two dimensional vector in (23) and $\mathbf{V}_{e,i} = (V_{xe,i}^{n+1/2}, V_{p_{xe,i}}^{n+1/2})$. Equation (23) for $\Delta_{\mathbf{X}e,i}$ is implicit and is solved iteratively: $\Delta_{\mathbf{X}e,i}^{k+1} = \frac{\Delta t}{2} \mathbf{V}_{e,i}(\mathbf{X}_{e,i} - \Delta_{\mathbf{X}e,i}^{k}, t_{n+1/2})$, where we start the iteration with $\Delta_{\mathbf{X}e,i}^{0}$=0 for *k*=0. Usually two or three iterations are sufficient to get a good convergence. The shifted values in Eq.(21,22) are calculated by a two-dimensional interpolation using a tensor product of cubic *B*-splines [13,14]. We now write that the distribution function is constant along the characteristics. Then $f_{e,i}^{n+1}$ is calculated from $f_{e,i}^{n}$ from the relation :

$$f_{e,i}^{n+1}(x_{j_x}, p_{xe,ij_p}) = f_{e,i}^{n}(x(t_n), p_{xe,i}(t_n)) = f_{e,i}^{n}(x - 2\Delta_{xe,i}, p_{xe,i} - 2\Delta_{p_{xe,i}}) \ ; \quad . \quad \textbf{(24)}$$

Again the shifted values in (24) are calculated with a two-dimensional interpolation using a tensor product of cubic *B*-splines.

Makar et al. Month. Wea. Review 124, 182 (1995)

Sonnendrücker et al. J. Comp. Phys. 149, 201 (1999)

Shoucri et al. Comp. Phys. Comm. 154, 65 (2003)

A circularly polarized laser beam incident on an overdense plasma: ion acceleration and plasma jet formation

$n / n_{cr} = 100$

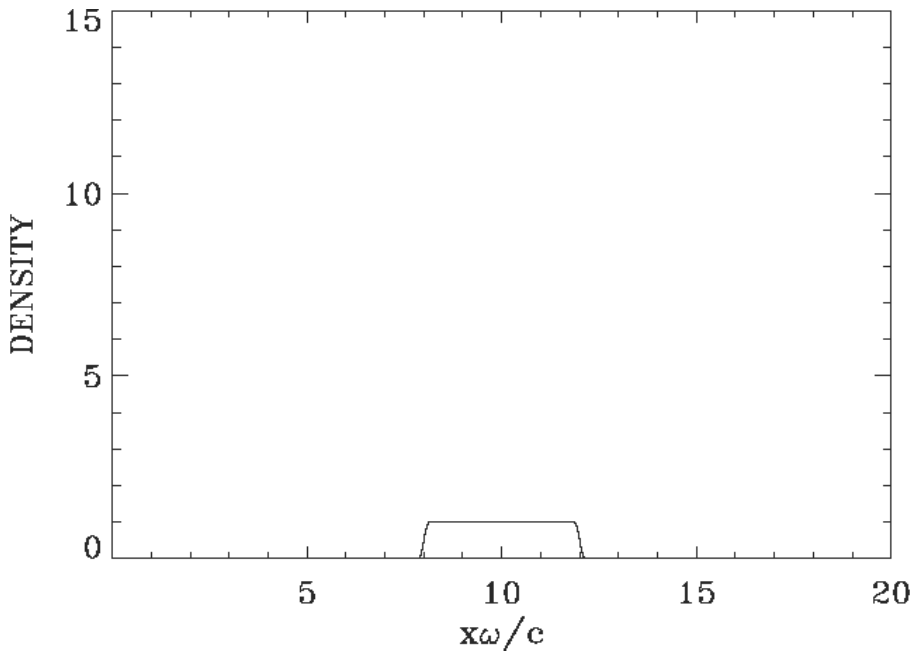

-**Time is normalized to** ω^{-1} **, and distance to** ω / c

-**The forward propagating circularly polarized laser wave enters the system at the left hand (x=0) boundary, where the forward propagating field**

$$E^{+} = 2E_0 P_r(t)\cos\tau \qquad F^{-} = -2E_0 P_r(t)\sin(\tau)$$

-**The shape factor** $P_r(t) = \exp(-2.\ln(2.)(\tau / t_p)^2)$ $\tau = t - 1.5t_p$ $t_p = 12$

-**Another case use** $P_r(t) = 1$ **for** $t > 1.5t_p$

-**A characteristic parameter of a high power laser beam is the normalized vector potential or quiver momentum** $|a_\perp| = |e\vec{A} / M_e c| = a_0$ **, where** $\vec{A}_\perp$ **is the vector potential of the wave. We choose for the amplitude of the potential vector** $a_0 = 25/\sqrt{2}$ **. For the circularly polarized wave** $2a_0^2 = I\lambda_0^2 / 1.368\text{x}10^{18}$ ***I*** **is the laser intensity in** $Watts / cm^2, \lambda_0$ **is the laser wavelength in microns.**

- $\omega = 0.1\omega_p$ **corresponding to** $n / n_{cr} = 100$

- **The lorentz factor for the oscillation of an electron in the field of the wave is** $\gamma_0 = \left(1 + a_0^2\right)^{1/2}$

- **The initial distribution functions for electrons and ion are Maxwellian with temperature *Te*=1.Kev for the electrons and for the ions *Ti*=0.1 Kev . *Mi/Me*=2.x1836**

- **We use a fine resolution in the phase-space, with *N*=10000 grid points in space and 2200 grid points in momemtum space for the electrons and the ions in the Vlasov code (extrema of the electron momentum are** ± 5**, and** ± 210 **for the ion momentum). This fine resolution of the phase-space guarantees accurate results. We use a time-step and a grid size such that** $\Delta t = \Delta x = 0.002$

- **The total length of the system is** $L = 20c / \omega$ **We have a vacuum region of length** $L_{vac} = 7.85c / \omega$ **on each side of the plasma slab. The steep jump in density at the plasma edge on each side of the flat top density of the slab target is** $L_{edge} = 0.3c / \omega$ **. The length of the central plasma slab with flat top density of 1 (normalized to** $100n_{cr}$ **) is** $L_p = 3.7c / \omega$ **. In free space** $\omega = k$ **for the electromagnetic wave , and** $\lambda_0 = 2\pi / k = 6.283$ **It follows that** $\lambda_0 >> L_{edge}$

The Vlasov code is executed on an Opteron 2218 processor (cpu 2.6 GHz). The PIC code is the relativistic 1D code BOPS, (Bourdier, 1983). It is executed on an AMD Opteron processor (cpu 2.19 GHz)

A circularly polarized laser beam normally incident on an overdense plasma (n/ncr=100): ion acceleration and plasma jet formation

THE CASE OF A CONSTANT LASER INTENSITY

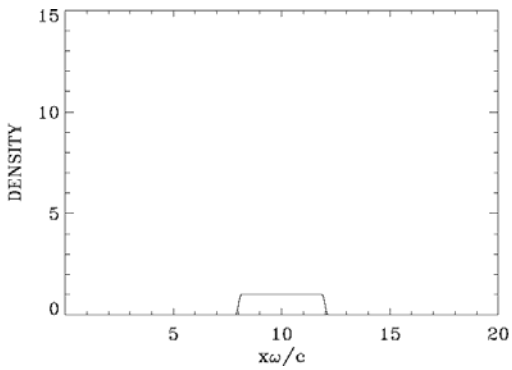

Fig.1a Electron (full curve) and ion (dashed curve) density profile at *t*=0.

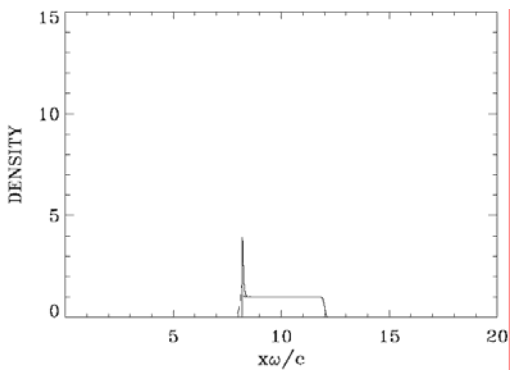

Fig.1b Electron (full curve) and ion (dashed curve) density profile at *t*=20

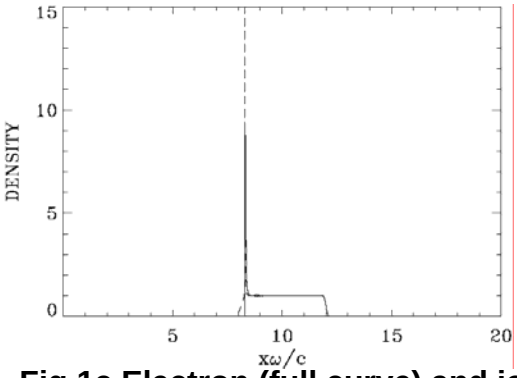

Fig.1c Electron (full curve) and ion (dashed curve) density profile at *t*=25. 2 (Vlasov code)

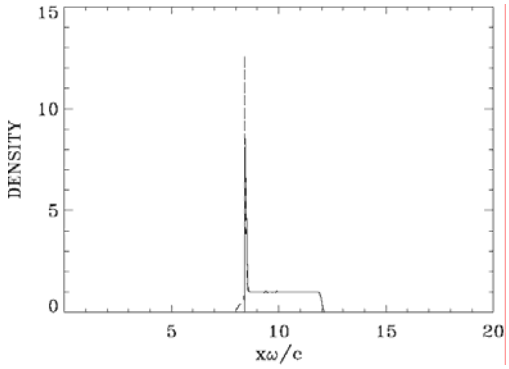

Fig.1d Electron (full curve) and ion (dashed curve) density profile at *t*=30. (Vlasov code)

Fig.1e Electron (full curve) and ion (dashedcurve) density profile at *t*=55. (Vlasov code)

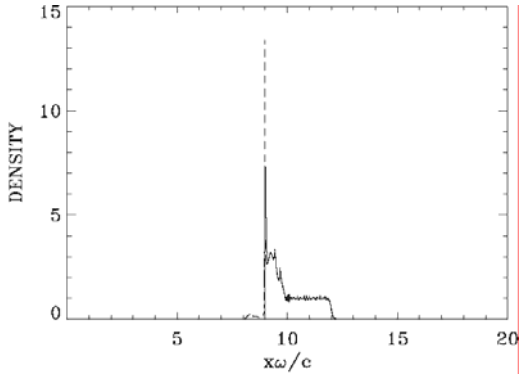

VLASOV CODE

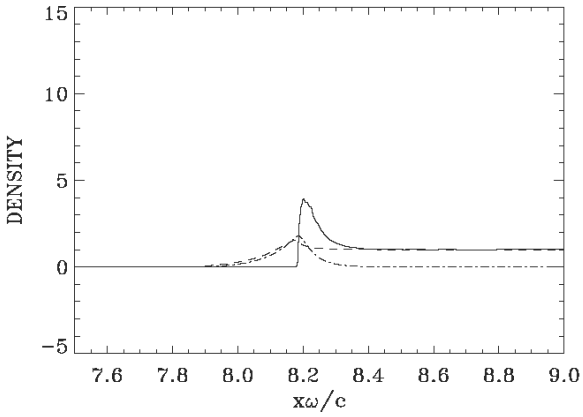

Fig.2a Density profiles at the edge of the plasma for the electrons (full curve), the ions (dashed curve) and the electric field (dashed-dotted curve), *t*=20 (same as Fig.(1b)). (Vlasov cc

PIC CODE

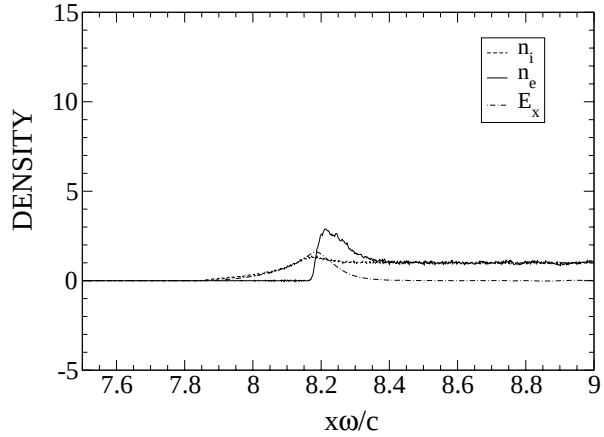

Fig.3a Density profiles at the edge of the plasma for the electrons (full curve), the ions (dashed curve) and the electric field (dashed-dotted curve), *t*=20.0

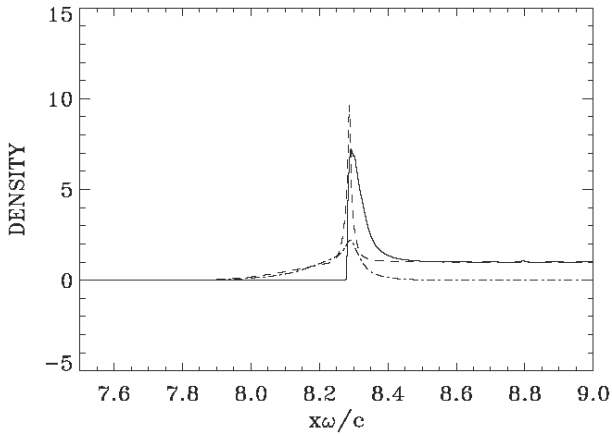

Fig.2b t=24.4 (Vlasov code)

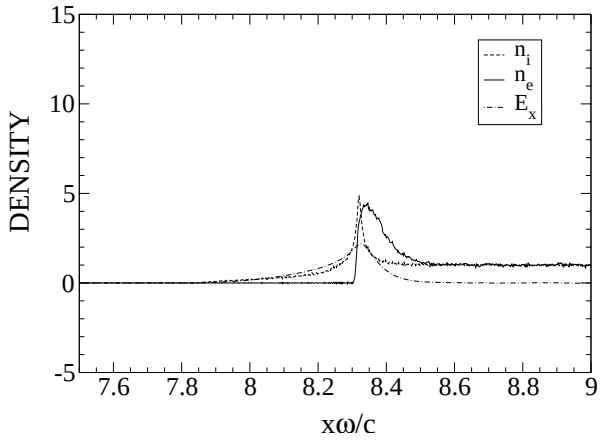

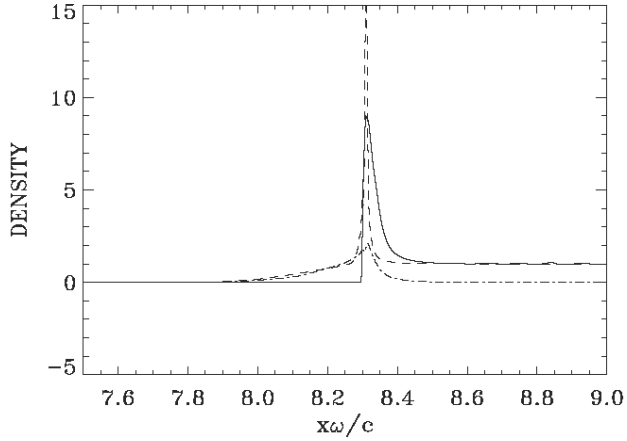

Fig.2c t=25.2 (Vlasov code)

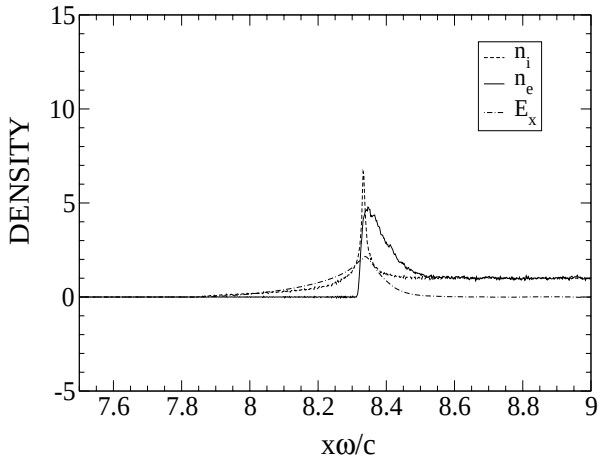

Fig.3c t=25.6 (PIC code)

VLASOV CODE **PIC CODE**

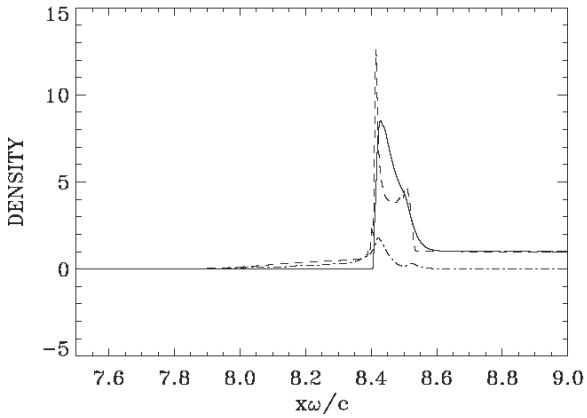

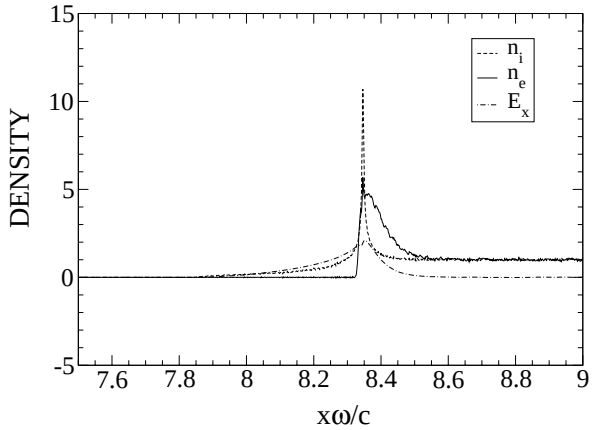

Fig.2d t=30 (Vlasov code)

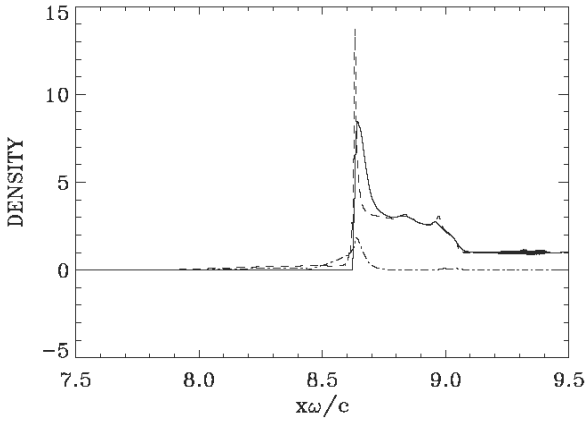

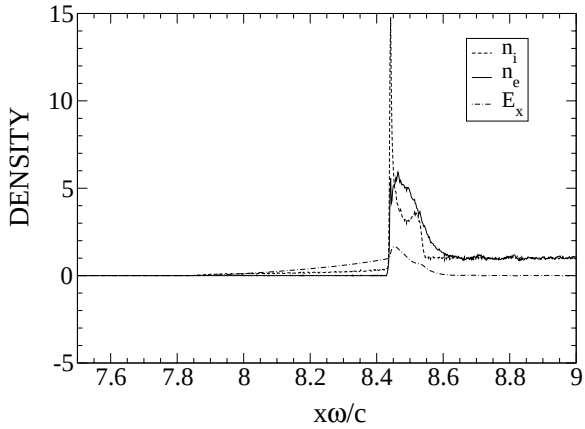

Fig.2e t=40 (Vlasov code)

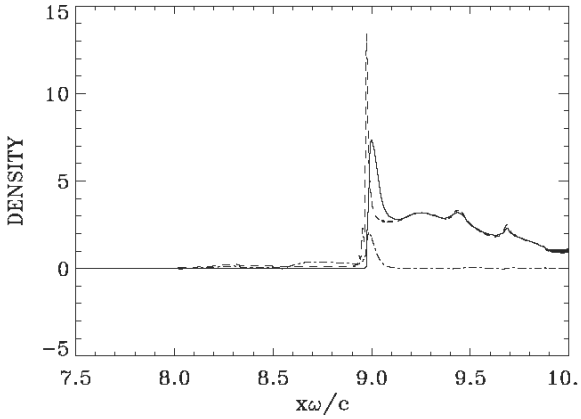

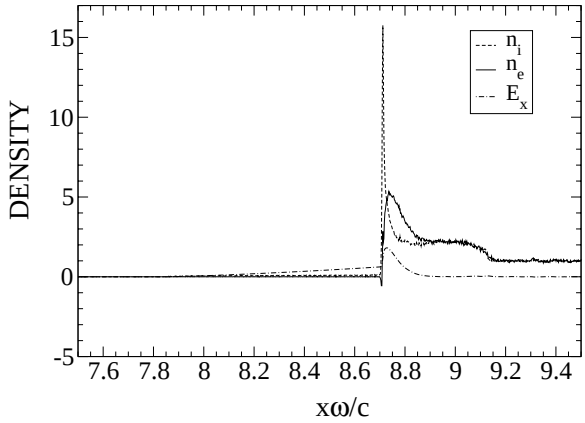

Fig.3e t=55 (Vlasov code) Fig.3f t=40 (PIC code)

ELECTROMAGNETIC WAVE FIELD

$$E^{\pm} = E_y \pm B_z$$

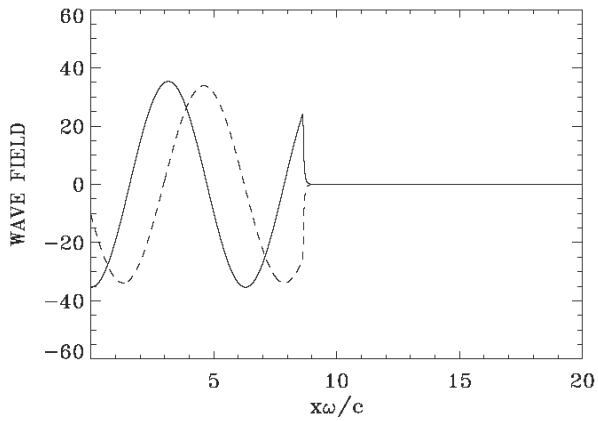

Fig.4a Incident wave E^{+} (full curve) and reflected wave E^{-} (dashed curve), t=40 (Vlasov code)

$$F^{\pm} = E_z \pm B_y$$

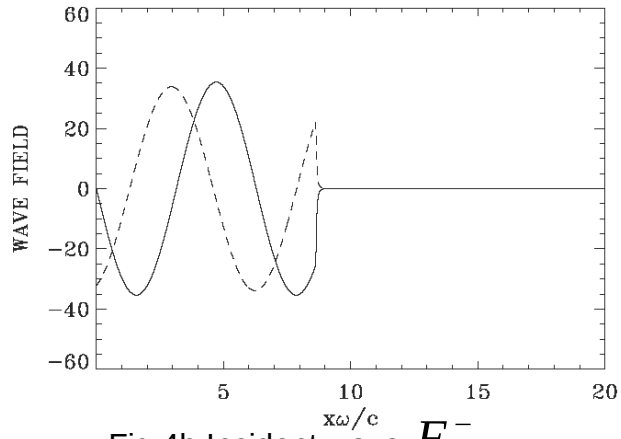

Fig.4b Incident wave F^{-} (full curve) and reflected wave F^{+} (dashed curve), t=40 (Vlasov code)

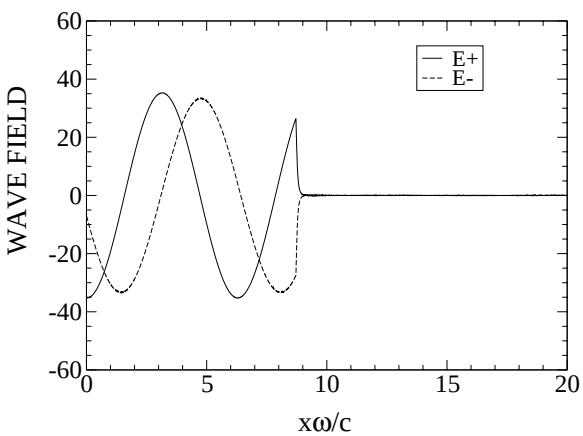

(PIC code)

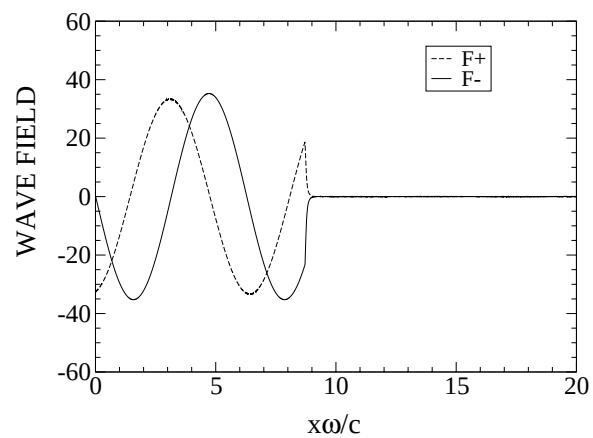

(PIC code)

Figure 4a presents the forward propagating wave E^+(full curve) and the backward reflected wave E^- (dashed curve) at *t*=40 for the calculation done with the Eulerian Vlasov code. Figure 4b presents the corresponding results for the forward propagating wave F^- (full curve) and the backward propagating wave F^+ (dashed-curve). The same results obtained from the PIC code are presented in Figures 5a,b. The agreement between the two codes for the phase and amplitude of the incident and reflected waves is excellent. The electromagnetic wave damps in the plasma over a distance of the order of the skin depth c/ω_{pe}. The strong increase of the ion and electron densities at the wave-front plasma-edge interface makes the plasma more opaque, with the steep plasma edge acting as a moving mirror for the incident light. Note that when E^+ is at a peak value, F^- is zero and vice-versa, so the wave is always maintaining a pressure on the surface of the plasma.The frequency of the backward reflected wave is slightly down-shifted by the moving reflecting plasma surface, which is acting as a mirror. We can check in Figures 4a,5a at *t*=40 the reflected waves (dashed curves) in vacuum have a wavelength (and a period) slightly bigger than the corresponding ones for the incident wave (full curve). In Guérin *et al*.,1996 the following analytical expressions were derived for the reflected wavenumber k_r and the reflected frequency ω_r of the laser wave due to the Doppler shift by the moving reflecting surface:

- $$\frac{\omega_r}{\omega} = \frac{1+\beta_F^2 - 2\beta_F/\beta}{1-\beta_F^2} \qquad \textbf{(a)}$$

- $$\frac{k_r}{k} = \frac{1+\beta_F^2 - 2\beta_F\beta}{1-\beta_F^2} \qquad \textbf{(b)}$$

where in our units $\beta_F = u_i = 0.024$ is the normalized velocity of the discontinuity surface, and $\beta = \omega/k = 1$ for the incident wave, since $\omega = k = 1$ for the incident laser wave in free space. We get for the reflected wave in free space from Eqs.(a-b), $\omega_r/\omega = k_r/k \approx 0.953$ or $\omega_r = k_r = 0.953$ since $\omega = k = 1$. This is confirmed if we follow the peaks of the reflected wave in Figures 4,5 (dashed-curves). We find a wavelength for the reflected wave of 6.562, which corresponds to $k_r \approx 0.957$, in close agreement to what is calculated from Eq.(b).

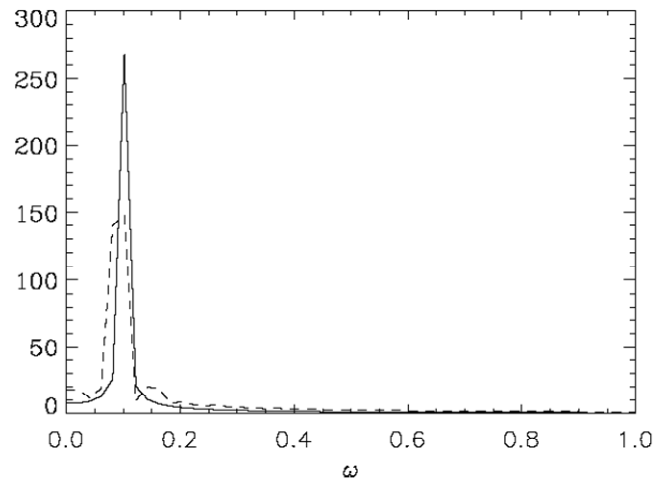

Fig.13 Frequency spectrum of the incident wave E^+ (full curve) and reflected wave E^- (dash curve), monitored at *x*=0

$n_{cr} = 1.1\frac{10^{21}}{\lambda_0^2}$ **cm^{-3}**

$n = 100\ n_{cr}$

at $\lambda_0 = 1\mu m$ **we have** $\omega_p = 5.64\text{x}10^4\sqrt{n} = 1.871\text{x}10^{16}$ **cm^{-3}**

$$\frac{c}{\omega_p} = 16\,nm$$

Length of the system considered $L_p = 20c/\omega = 200c/\omega_p$ **=3200nm**

at $\lambda_0 = 1\mu m$ **, period in free space =3.3 femtsec.**

Period of the wave $T = \frac{2\pi}{\omega} = 6.283\omega^{-1}$

T=40 corresponds to 40/6.283=6.366 periods or 21 femtsec

$P_r(t) = \exp(-2.\ln(2.)(\tau/t_p)^2)$ **tp=12 6.3 femtsec**

$\tau = t - 1.5t_p$ **18 9.454 femtsec**

PHASE-SPACE ION DISTRIBUTION FUNCTION

VLASOV CODE **PIC CODE**

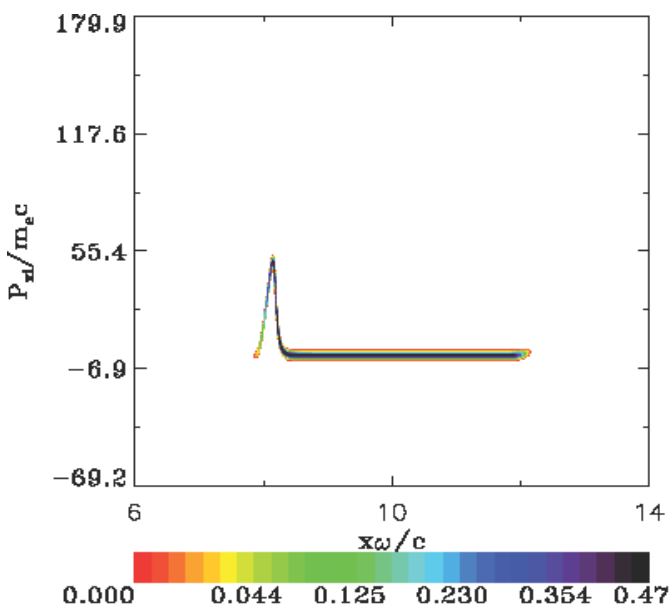

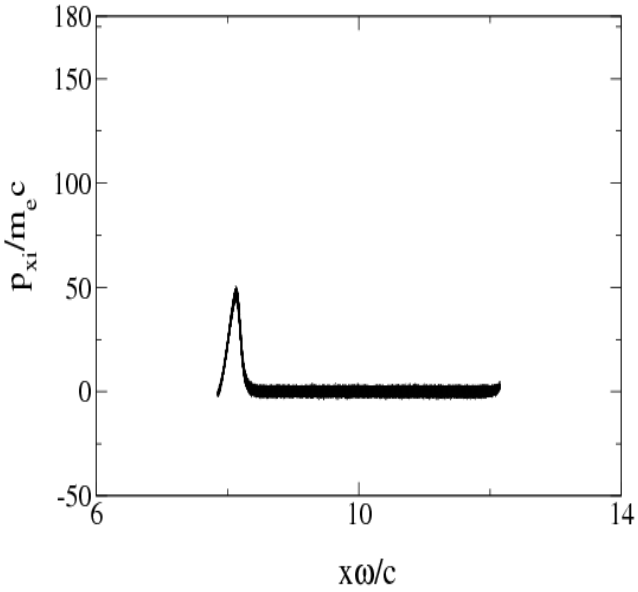

Fig.6a Phase-space plot of the ion distribution function at *t*=20

VLASOV CODE **PIC CODE**

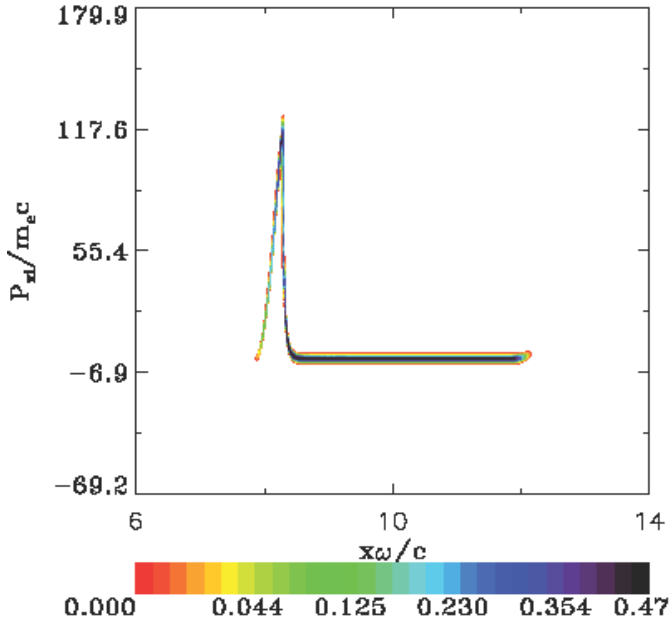

Fig.6b Phase-space plot of the ion distribution function at t=24.4 Vlasov code

PHASE-SPACE ION DISTRIBUTION FUNCTION

VLASOV CODE **PIC CODE**

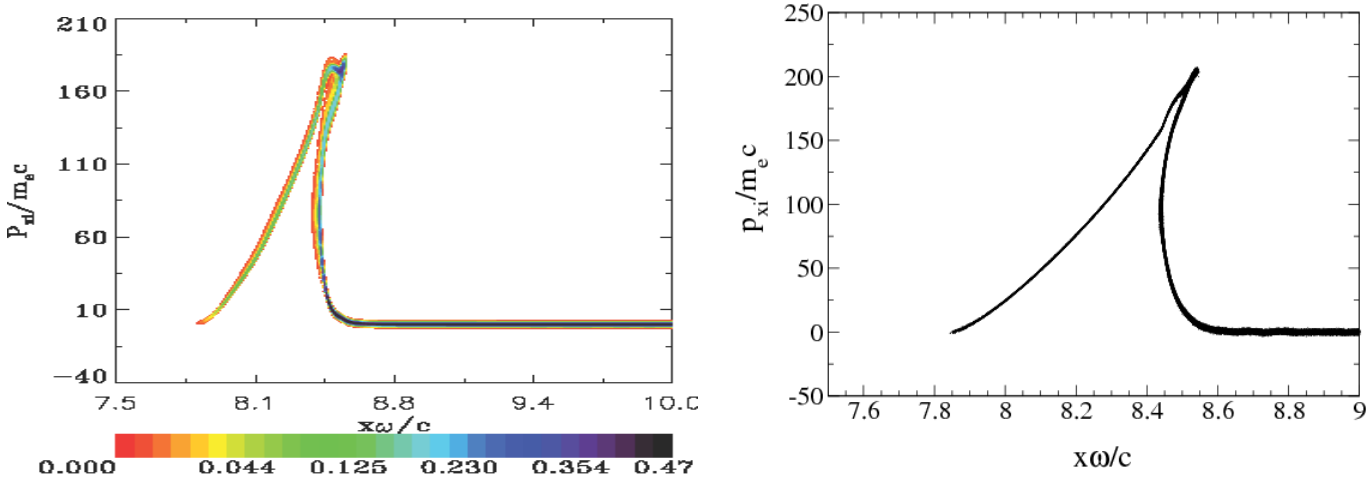

Fig.6c Phase-space plot of the ion distribution function at *t*=30

VLASOV CODE **PIC CODE**

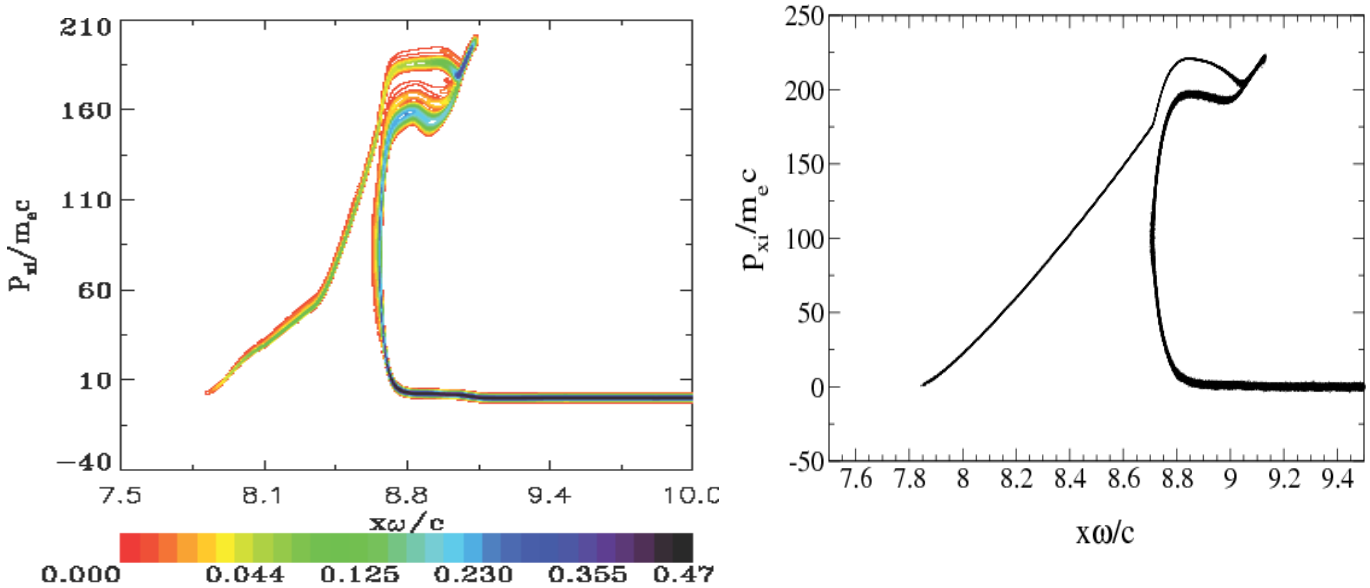

Fig.6d Phase-space plot of the ion distribution function at *t*=40

VLASOV CODE **PIC CODE**

PHASE-SPACE ION DISTRIBUTION FUNCTION
VLASOV CODE

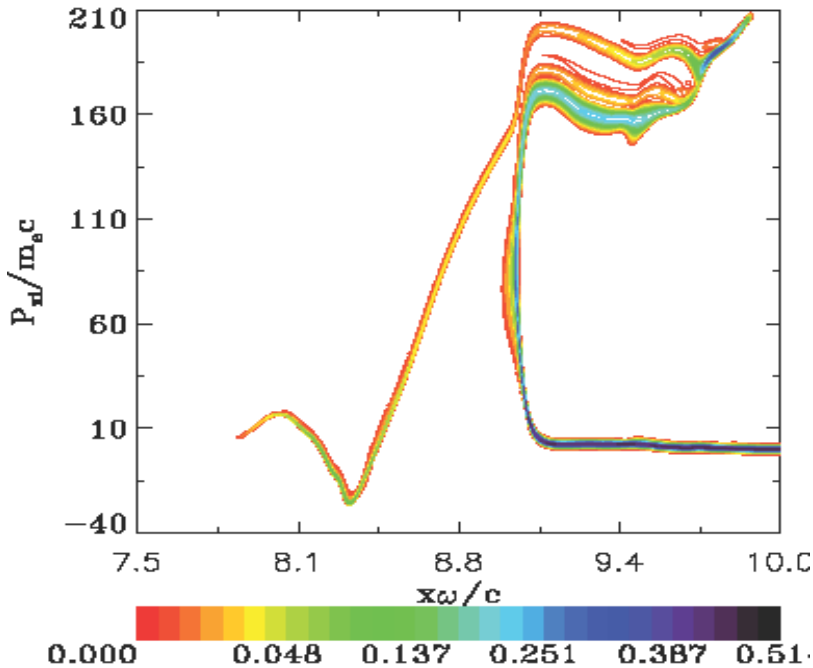

Fig.6e Phase-space plot of the ion distribution function at t=55 (Vlasov code)

PHASE-SPACE DISTRIBUTION FUNCTION FOR THE ELECTRONS (PIC CODE)

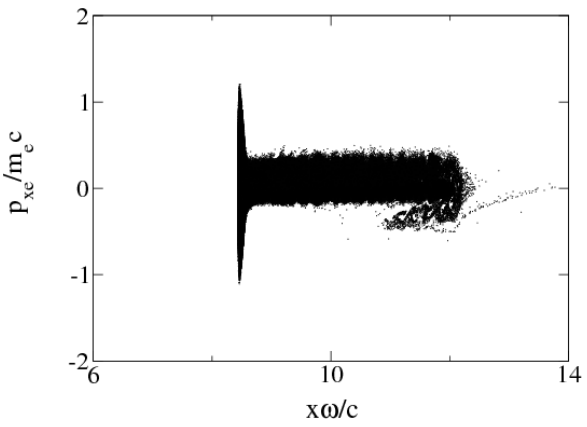

Fig.8a Phase-space plot of the electron distribution function *t*=30

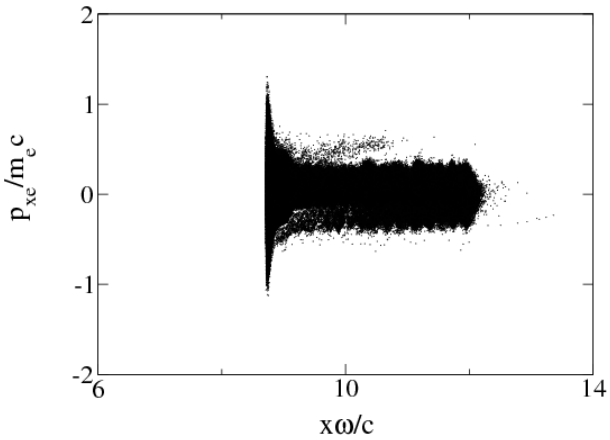

Fig.8b Phase-space plot of the electron distribution function t=40

PHASE-SPACE ELECTRON DISTRIBUTION FUNCTION (VLASOV CODE)

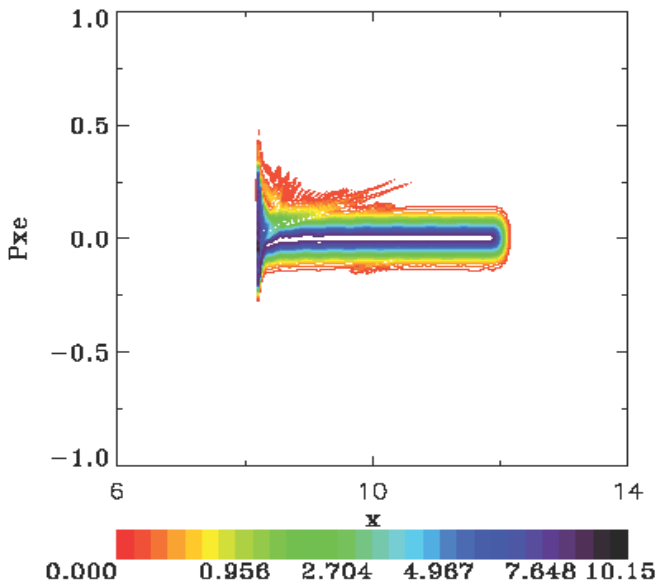

Fig.9a Phase-space plot of the electron distribution function *t*=20

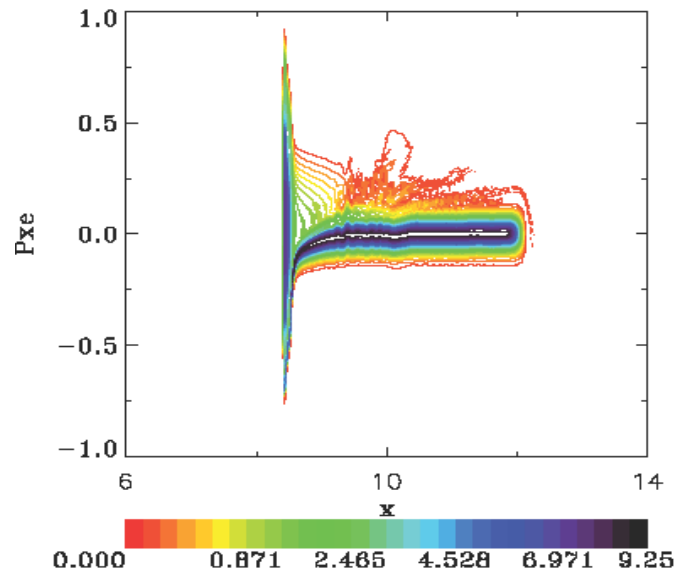

Fig.9b Phase-space plot of the electron distribution function *t*=30

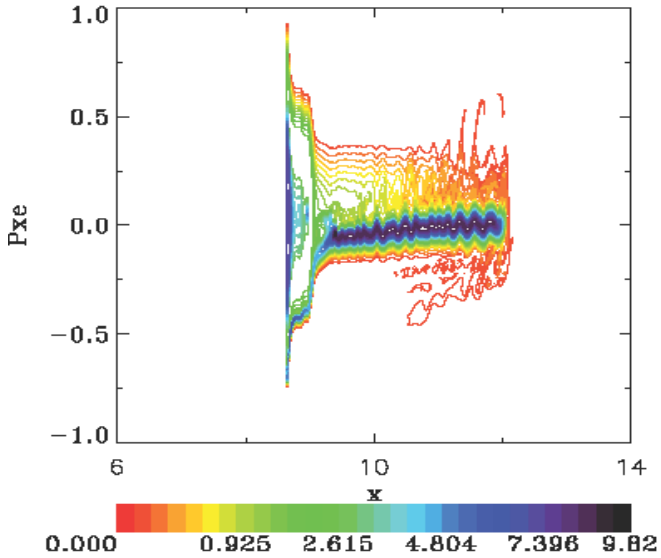

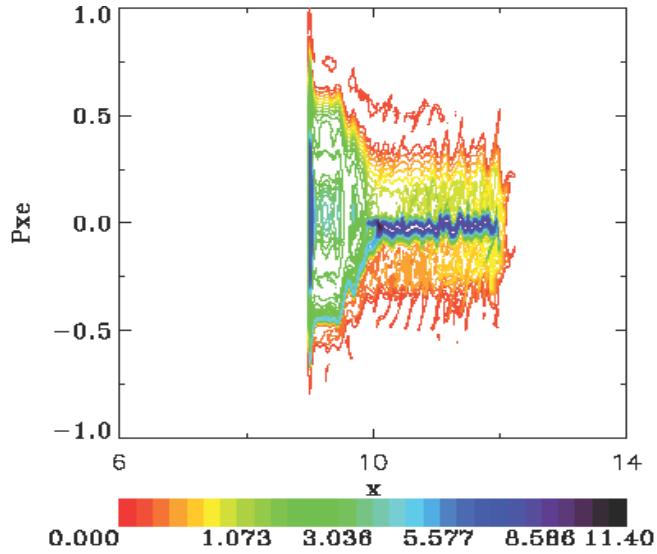

Fig.9c *t*=40 (Vlasov code) Fig.9d *t*=55

PHASE-SPACE ELECTRON DISTRIBUTION FUNCTION (VLASOV CODE)

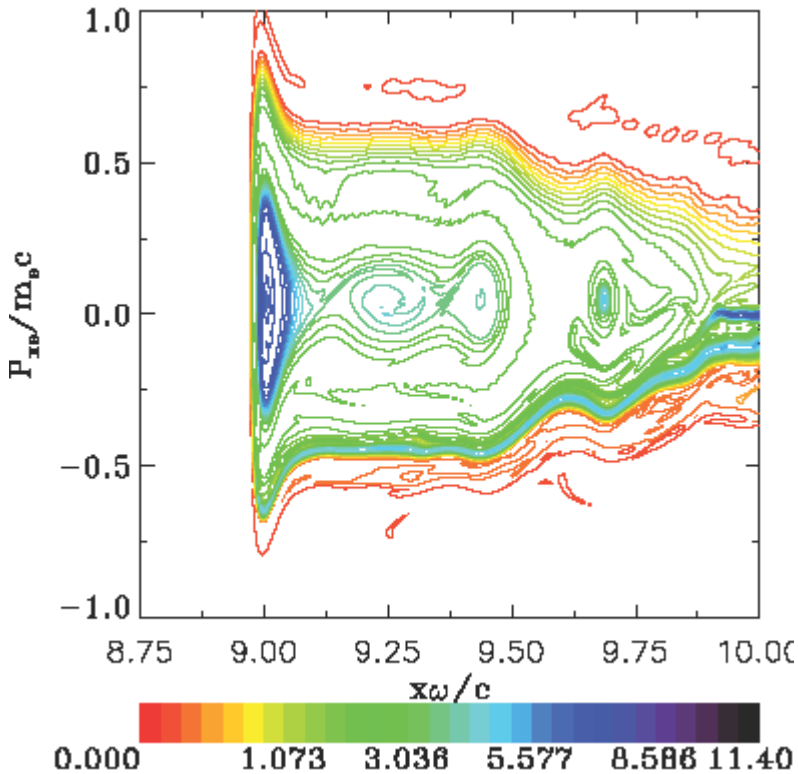

Fig.10 Same as Fig.(9d), phase-space plot of the electron distribution function at *t*=55, concentrating on the edge region (Vlasov code)

- **The position of the wave-front plasma-edge interface and the solitary-like structure of the ions in Figure 2 (Vlasov code) and Figure 3 (PIC code) are essentially the same (the solitary ion peak in Figure 2e is at *x*=8.64 and in Figure 3f at *x*=8.7). This interface is traveling at a constant speed for *t*>18 under the constant ponderomotive pressure of the incident laser beam. This constant speed is calculated from the numerical results by following the interface in Figure 2 or Figure 3, and has a value of 0.024. The velocity of the front pushed by the ponderomotive pressure was calculated in Denavit,1992 by balancing the electromagnetic pressure at the absorber surface with the rate of increase in ion momentum, and the following expression for the velocity of the surface of discontinuity was obtained:**
- $$u_i = a_0 \left(\frac{n_c}{n} \frac{M_e}{M_i} \right)^{1/2} \qquad \textbf{(16)}$$
-
- **With ,** $a_0 = 25/\sqrt{2}$ **and** $n/n_c = 100$**,** $M_e/M_i = 0.5/1836$ **we calculate** $u_i = 0.029$ **(normalized to the velocity of light). This value is close to the value of 0.024 calculated by the Eulerian and the PIC codes. We note however a more accurate agreement with (16) obtained for more moderate values of** a_0 **used in Shoucri and Afeyan, 2010 and Shoucri, 2010 (where we used hydrogen, which resulted in a higher velocity). In the present case with deuterium, we have a smaller value of 0.024 for the velocity, and the margin of error for the accurate calculation of this small velocity can be bigger. (We note that the relativistic correction to Eq.(16) as reported by Schlegel et al., 2009 and Robinson et al., 2009 is small in our case and reduces the velocity calculated in Eq.(16) from 0.029 to 0.028).**

- **At the right of the ion peak in Figures 2d-f and Figures 3e-f we have a neutral plasma jet with a shock-like structure expanding to the right with an average speed of about 0.052, calculated by dividing the distance traveled by the neutral plasma edge by the corresponding time difference. This entire structure is stable as it propagates and expands to the right. The value of the free streaming edge at the right can also be calculated for the Eulerian Vlasov code from Figures 6d,e for instance, where we see the free streaming deuterium ions having a normalized momentum around 180. Hence**
- $M_i \upsilon / M_e c \approx 180$ **,or** $\upsilon / c \approx 180/(2.*1836)$ **= 0.05. This corresponds to an energy of the deuterium ions of** $M_i \upsilon^2 / 2 \approx M_i c^2 (\upsilon / c)^2 \approx 938\text{x}0.0025 = 2.345$ **MeV. The value obtained from the PIC code (Figure 7c) is slightly higher, we have** $M_i \upsilon / M_e c \approx 200$ **, or** $\upsilon / c \approx 200/(2.*1836)$ **=0.054.**

A CIRCULARLY POLARIZED LASER BEAM NORMALLY INCIDENT ON AN OVERDENSE PLASMA (n/Ncr=100): ION ACCELERATION AND PLASMA JET FORMATION
THE CASE OF A LASER BEAM PULSE

$$E^{+} = 2E_0 P_r(t)\cos\tau \qquad F^{-} = -2E_0 P_r(t)\sin(\tau)$$

$$P_r(t) = \exp(-2.\ln(2.)(\tau / t_p)^2) \quad \tau$$

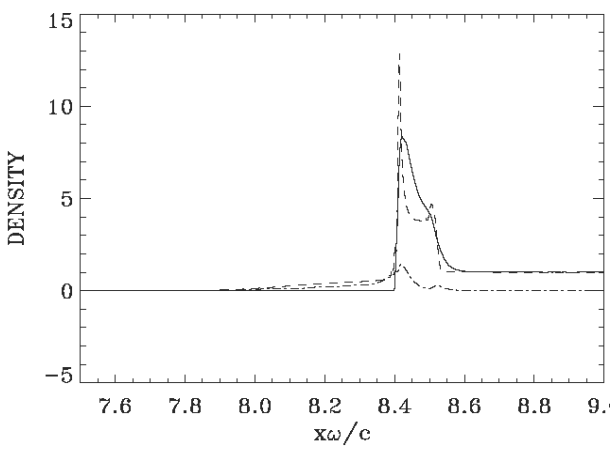

Fig.11a Density profiles at the edge of plasma for the electrons (full curve), the ions (dashed curve) and the electric field (dashed-dotted curve), *t*=30 (Vlasov code)

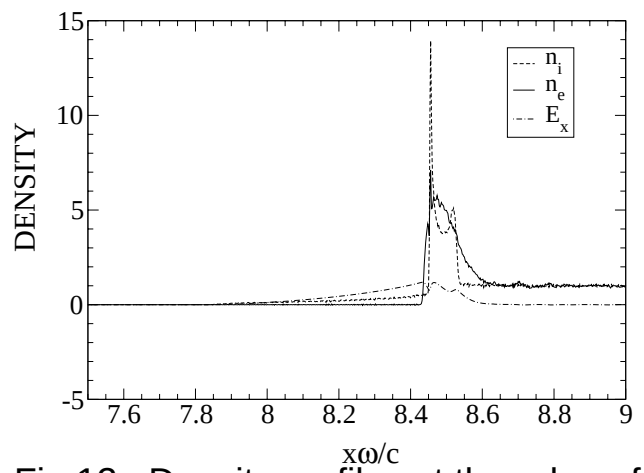

Fig.12a Density profiles at the edge of the plasma for the electrons (full curve), the ions (dashed curve) and the electric field (dashed-dotted curve), *t*=30

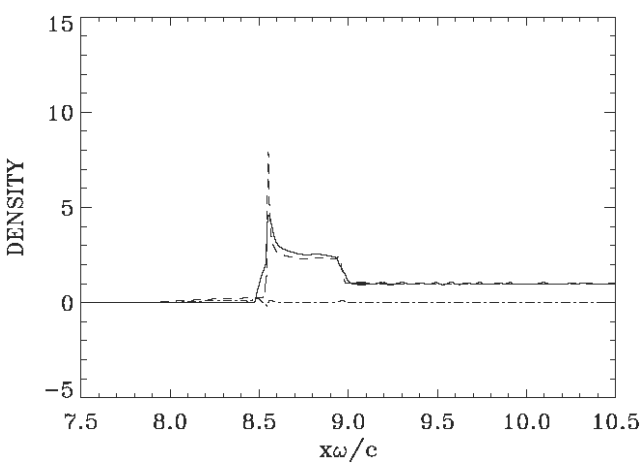

Fig.11b *t*=40 (Vlasov code)

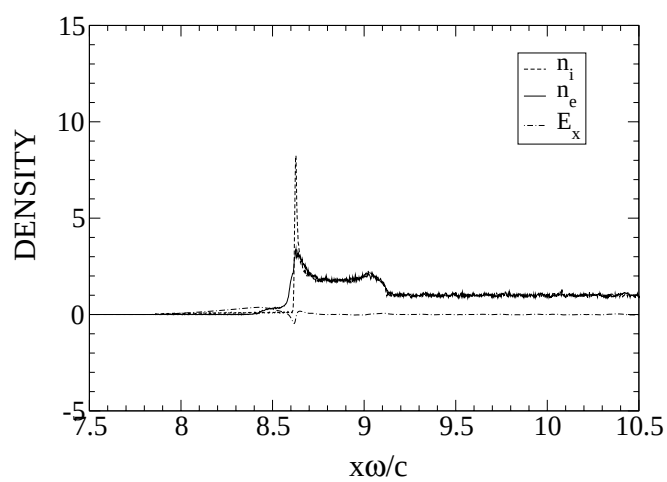

Fig.12b *t*=40 (PIC code)

VLASOV CODE **PIC CODE**

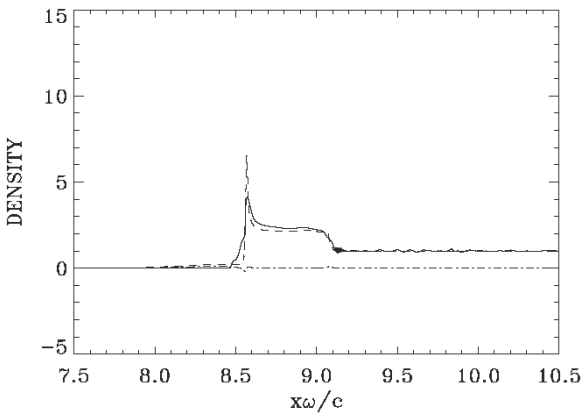

Fig.11c *t*=42.6 (Vlasov code)

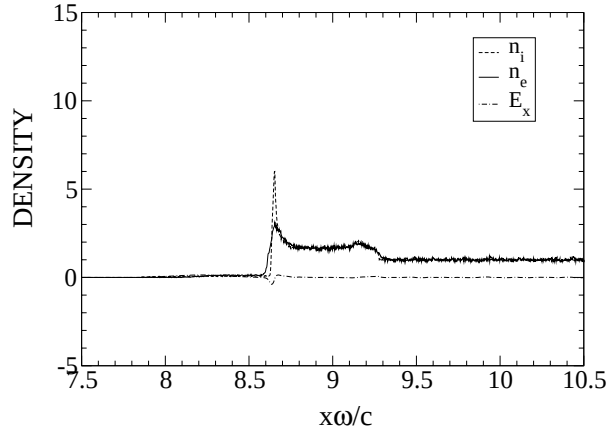

Fig.12c *t*=42.6 (PIC code)

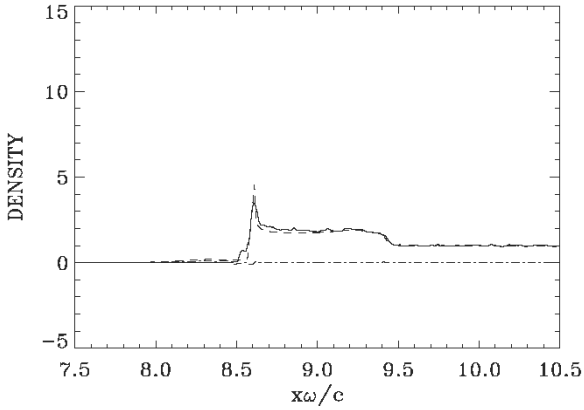

Fig.11d *t*=50. (Vlasov code)

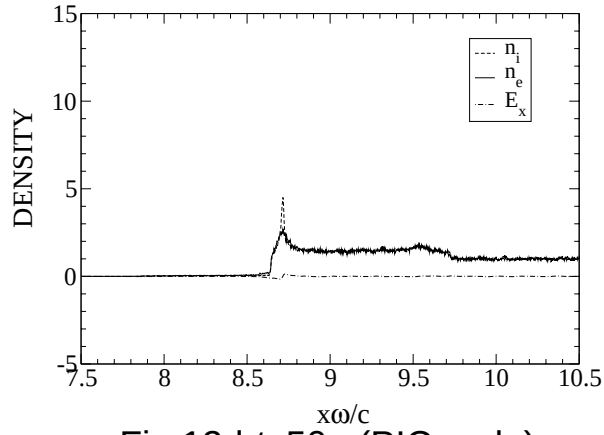

Fig.12d *t*=50. (PIC code)

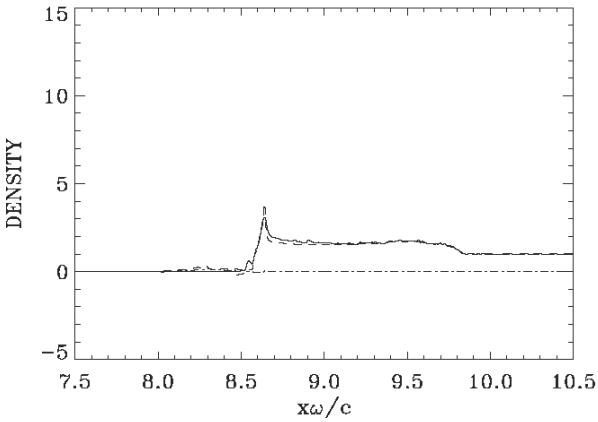

Fig.11e *t*=57.5 (Vlasov code)

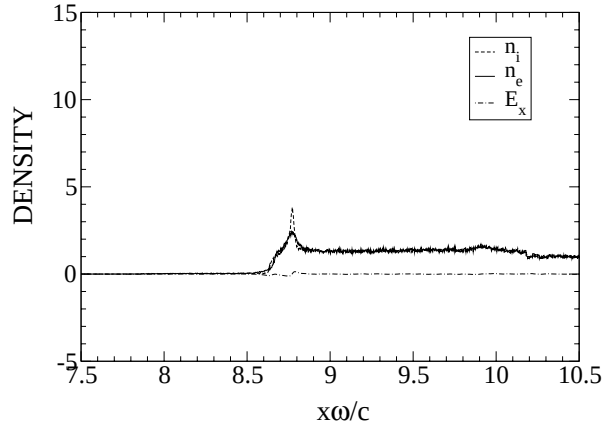

Fig.12e *t*=57.5 (PIC code)

ELECTRIC FIELD AT THE PLASMA EDGE
GAUSSIAN LASER BEAM PULSE
VLASOV CODE

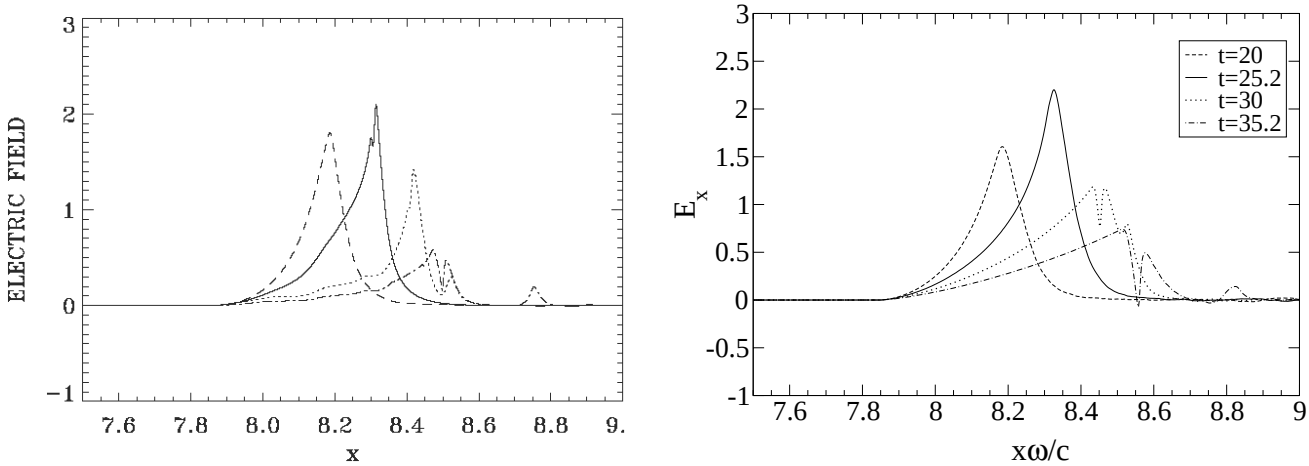

Fig.13 Electric field at the wave-front plasma-edge interface, at *t*=20, 25.2, 30, 35.2

ION PHASE-SPACE

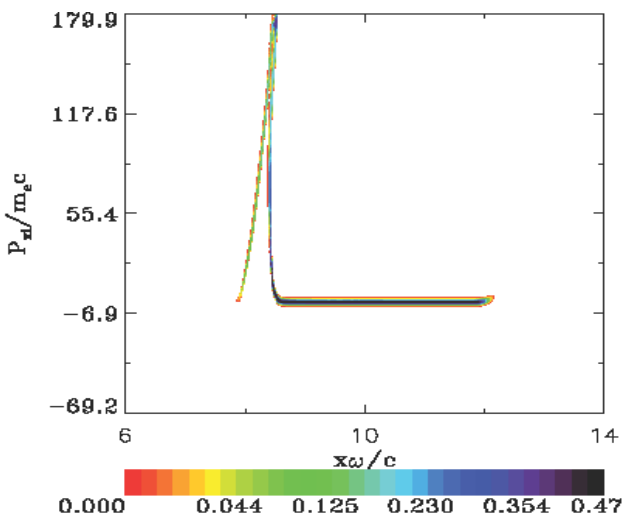

Fig.14a Phase-space plot of the ion distribution function *t*=30 (Vlasov code)

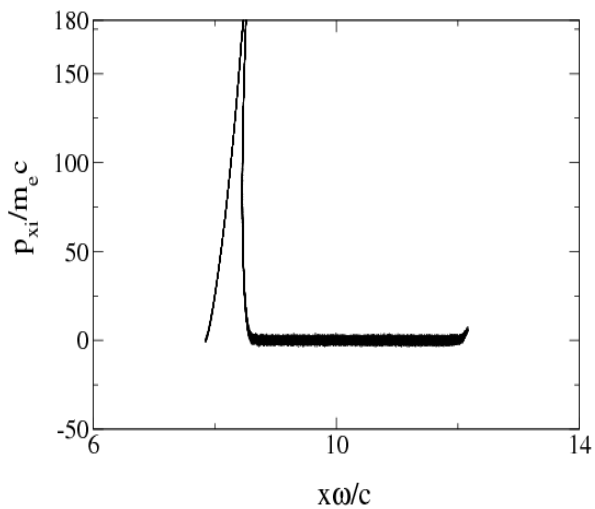

Fig.15a Phase-space plot of the ion distribution function *t*=30 (PIC code)

ION PHASE-SPACE

VLASOV CODE | **PIC CODE**

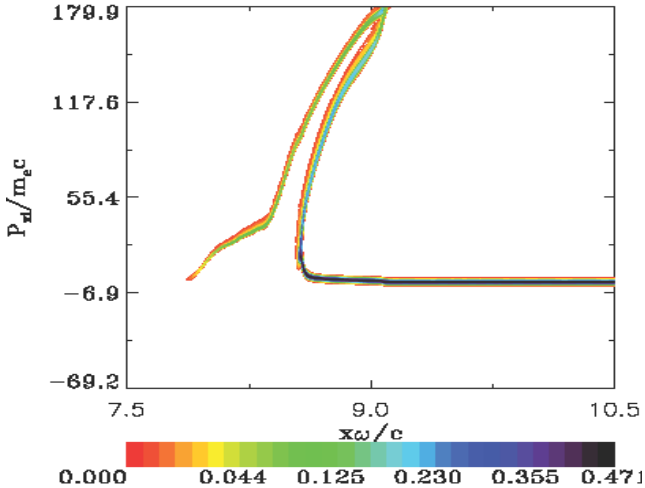

Fig.14b t-42.6 (Vlasov code)

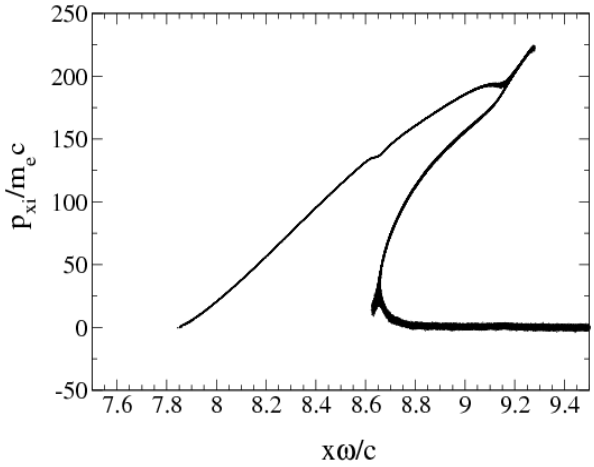

Fig.15b t=42.6 (PIC code)

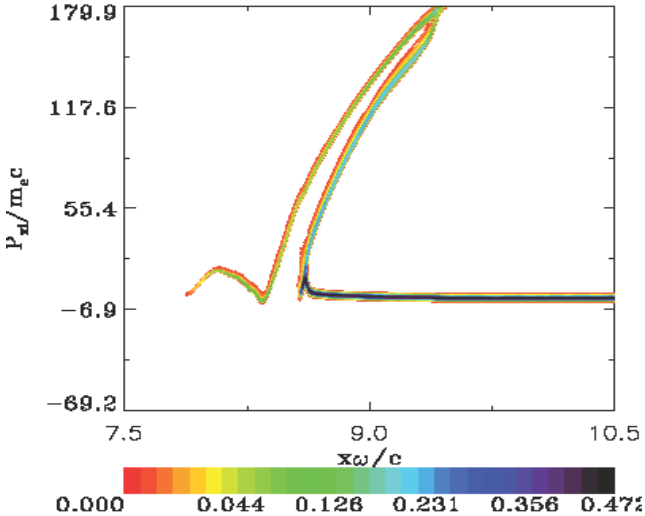

Fig.14b *t*-50. (Vlasov code)

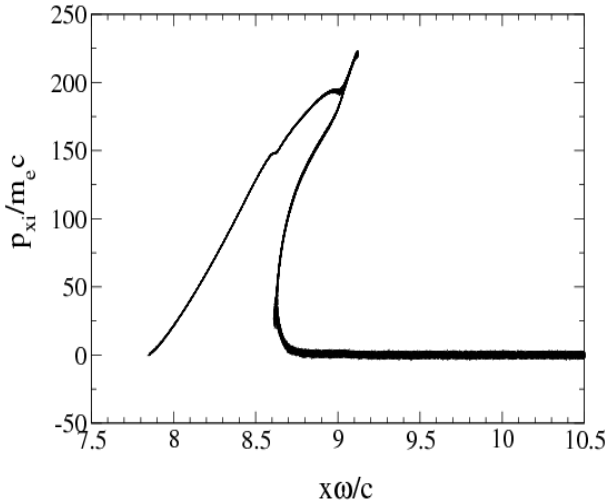

Fig.15b *t*=50. (PIC code)

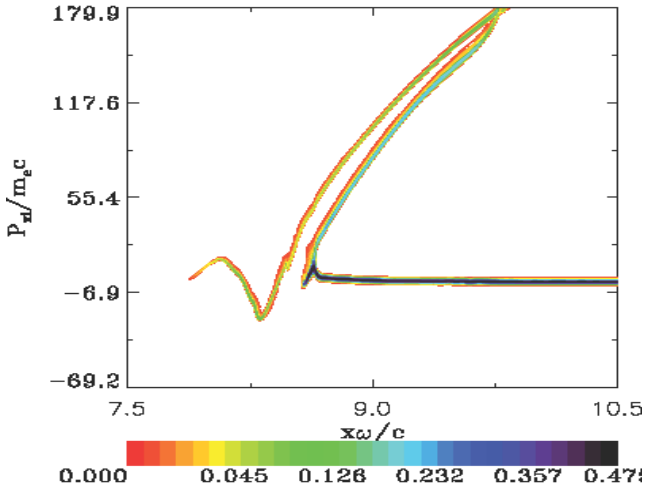

Fig.14b *t*-57.5 (Vlasov code)

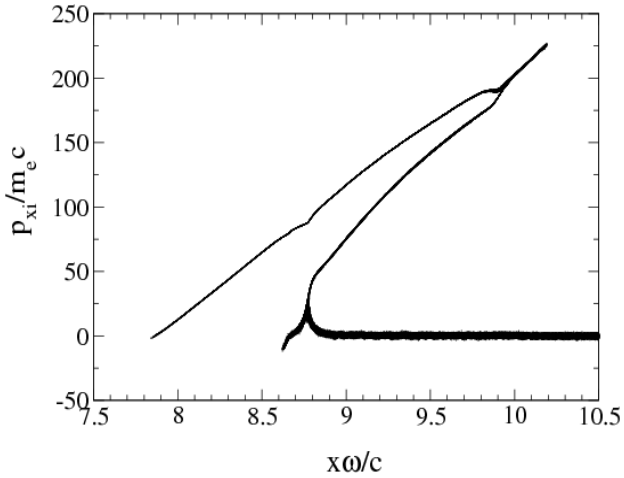

Fig.15b *t*=57.5 (PIC code)

ELECTRON PHASE-SPACE
VLASOV CODE
GAUSSIAN LASER BEAM PULSE

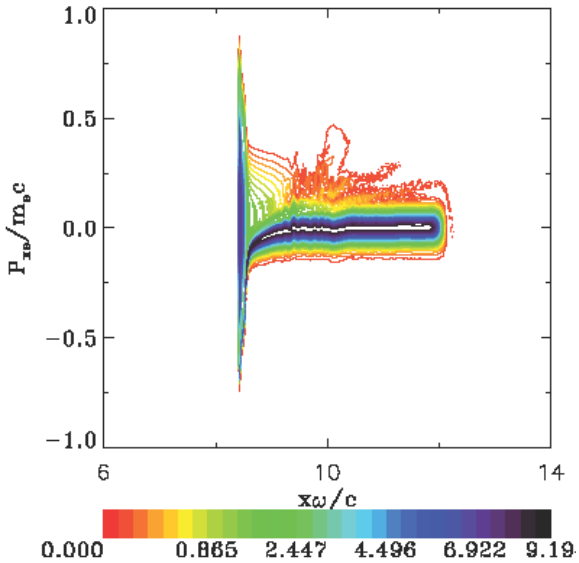

Fig.16a Phase-space plot of the electron distribution function at *t*=30

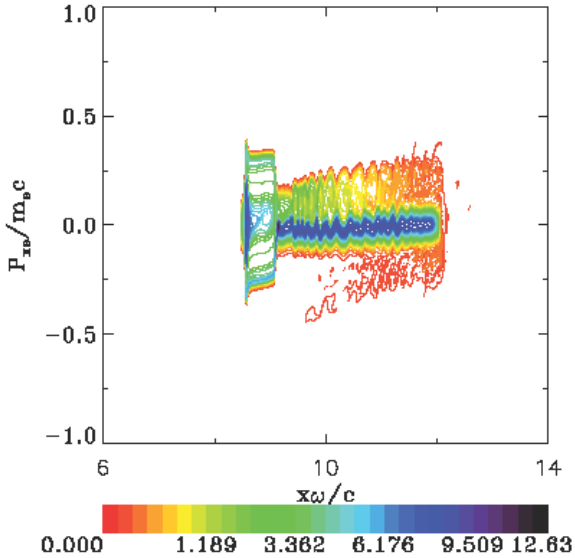

Fig.16b Phase-space plot of the electron distribution function at *t*=42.6

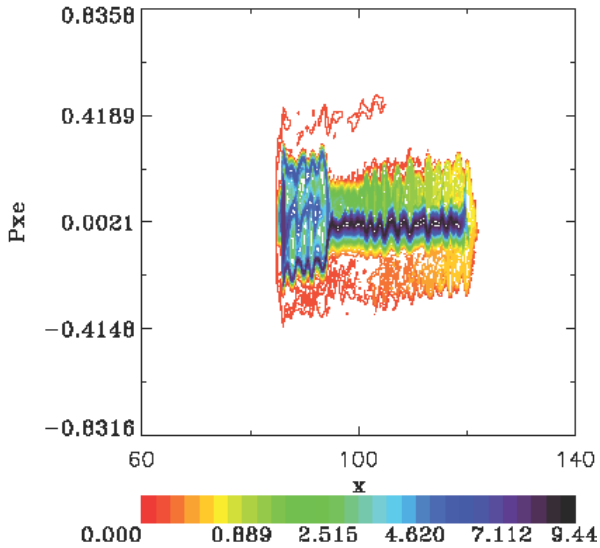

Fig.16c Phase-space plot of the electron distribution function at *t*=50

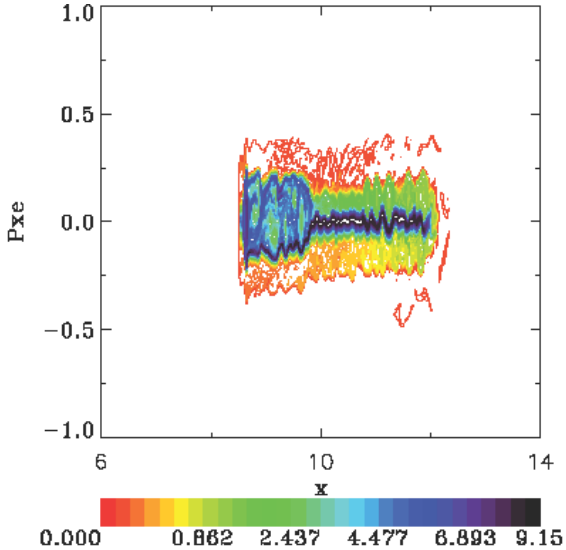

Fig.16d Phase-space plot of the electron distribution function at *t*=57.5

ELECTRON PHASE-SPACE
VLASOV CODE
GAUSSIAN LASER BEAM PULSE

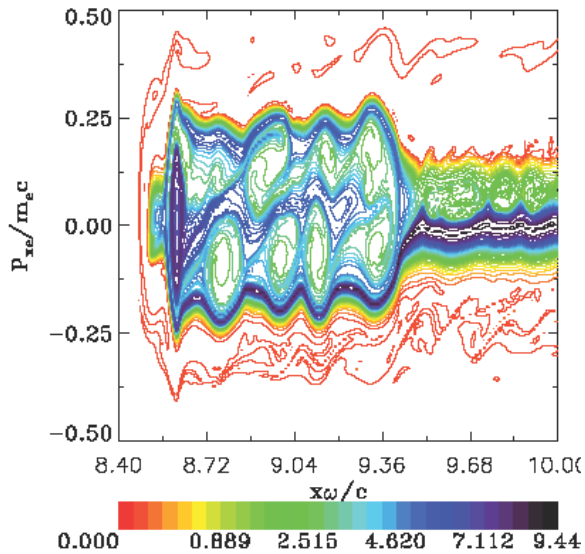

Fig.17a Phase-space plot of the electron distribution function (same as Fig.16c, concentrating on the expanding neutral plasma region)

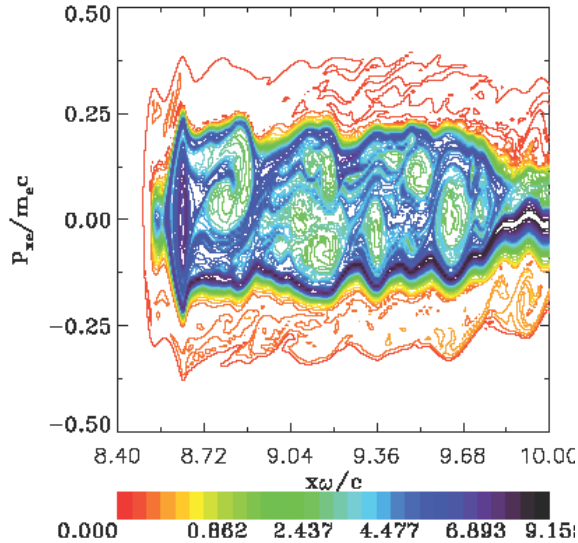

Fig.16b Phase-space plot of the electron distribution function (same as Fig.16d, concentrating on the expanding neutral plasma region

ELECTRON PHASE-SPACE
PIC CODE
GAUSSIAN LASER BEAM PULSE

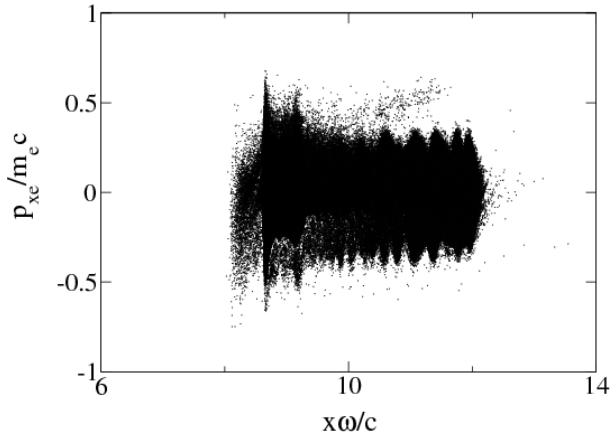

Fig.18a Phase-space plot of the electron distribution function at *t*=42.6 (PIC code)

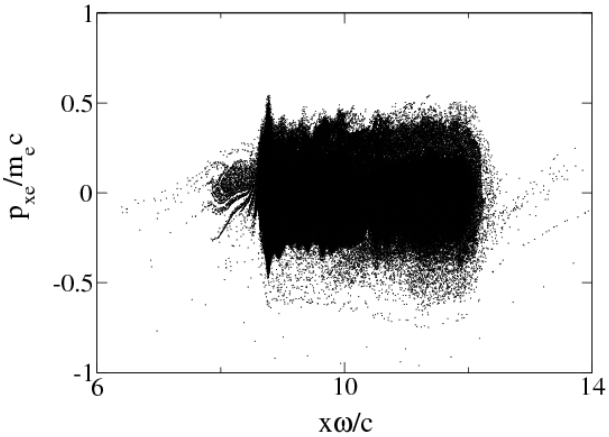

Fig.18b Phase-space plot of the electron distribution function at *t*=57.5 (PIC code)

ELECTROMAGNETIC WAVE FIELD

$$E^{\pm} = E_y \pm B_z$$

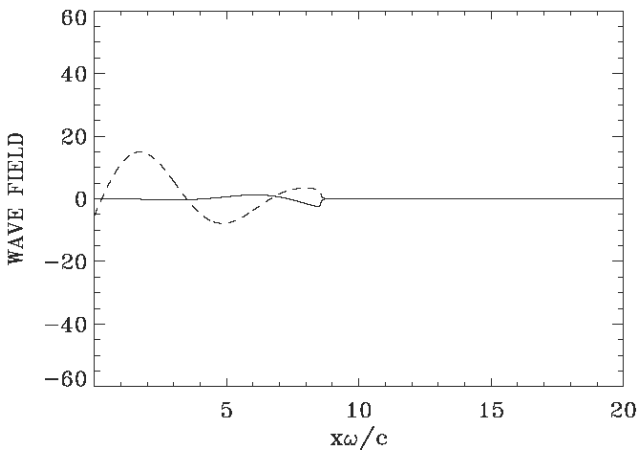

Fig.19a Incident wave E^{+} (full curve) and reflected wave E^{-} (dash curve) at t=42.6

$$F^{\pm} = E_z \pm B_y$$

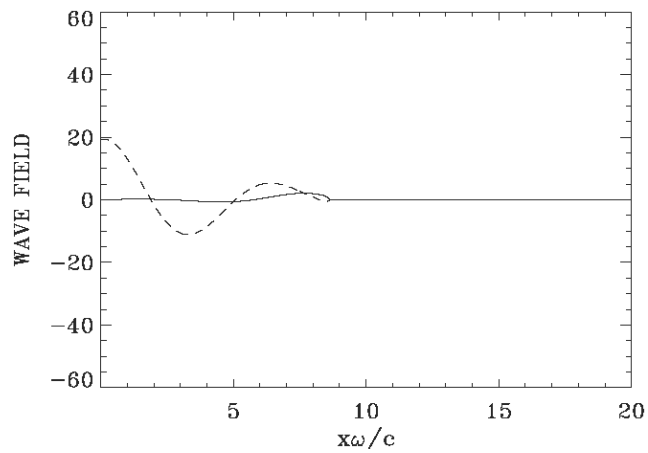

Fig.19b Incident wave F^{-} (full curve) and reflected wave F^{+} (dash curve) at t=42.6